Geochemistry of diabasic dikes and andesitic-basaltic lavas in Noorabad-Kermanshah ophiolite

Masoud Kiani[1], Ahmad Ahmadi-Khalaji[2], Zahra Kamali*[3], Hadi Shafaii Moghadam[4]

1- Department of Geology, Faculty of Sciences, Islamic Azad University, Science and Research Branch, Tehran, Iran.
2- Department of Geology, Faculty of Sciences, Lorestan University, Khorramabad, Iran.
3- School of Earth Sciences. Birjand University, Birjand, Iran.
4- School of Earth Sciences, Damghan University, Damghan, Iran.

* Corresponding Author: zahrakamali84@gmail.com

Received: 16 February 2014 / Accepted: 29 November 2014 / Published online: 1 January 2015

Abstract

The Noorabad-Kermanshah ophiolite is part of Eastern Mediterranean-Zagros-Oman Tethyan ophiolites, that this area is located in south-southwest of the Main Zagros Thrust fault. This ophiolite consists of peridotites, serpentinites and pegmatite gabbros as mantle sequence whereas crustal sequences are composed of locally layered gabbros, isotropic gabbros, sheeted dike complex, basaltic to andesitic lavas and sedimentary rocks (radiolarites and late Cretaceous pelagic limestones). The diabase dikes enriched in LREE relative to HREE elements($La_{(n)}/Yb_{(n)}$=1.7-3.3). Also, the andesites are enriched in LREE relative to HREE elements($La_{(n)}/Yb_{(n)}$=3.1-5.37) and the pillow lavas are enriched in LILE ($Th_{(n)}/La_{(n)}$=2.1) while show a depletion in HFSE ($Nb_{(n)}/La_{(n)}$=0.07-0.2). The Basaltic-andesitic lavas exhibiting mainly calc-alkaline, with minor island-arc tholeiitic affinities, are characterized by enrichment in LILE and LREE and depletion in HFSE. These geochemical characteristics compared with other Tethyan ophiolites along the Bitlis-Zagros suture zone reveal a supra-subduction zone environment for the genesis of the Noorabad-Kermanshah ophiolites.

Keywords: Diabasic dikes, Basaltic-andesitic lavas, Geochemistry, Supra-subduction zone, Noorabad ophiolites.

1–Introduction

The Tethyan ophiolites in the Alpine-Himalayan orogenic system are exposed along curvilinear suture zones, bounding a series of continental fragments of Gondwana (Dilek *et al*., 2008). The Jurassic ophiolites in the Alpine–Apennine mountain belt in the west (Fig.1) commonly display MORB geochemistry (Tribuzio *et al*.,1999; Rampone and Piccardo, 2000), while the Late Jurassic– Cretaceous ophiolites in the Tauride– Pontide (Turkey), Zagros (Iran), and Himalayan mountain belts to the east show geochemical affinities characteristic of suprasubduction zone (SSZ) environments (Pearce *et al*., 1981, 1984; Arvin, 1990;Robinson and Malpas, 1990; Hassanipak and Ghazi, 2000; Hebert and Laurent, 1989; Hébert *et al*., 2003; Malpas *et al*., 2003; Parlak *et al*., 2006; Dilek *et al*., 2008;ShafaiiMoghadam *et al*. 2011).The ophiolitic complexes along Bitlis-Zagros Suture Zone include: Baer-Bassit (Syria), Hatay, Kizildag, and Cilo (Turkey); Kermanshah, Neyriz and Esphandagheh (Iran), (e.g., Moores *et al*.,1984; Dilek and Delaloye, 1992; Dilek and Moores,1987).

The Zagros fold-and-thrust belt of Southwest Iran defines the central part of the peri-Arabian convergent margin and reflects the Oligo-Miocene closure of Neotethys (Shafaii Moghadam *et al*, 2012).The Zagros Suture Zone extends from the Turkey-Iran border to just north of the Straits of Hormuz that constitute the significant part of this orogenic belt .The ophiolites from Iran may be classified into two groups, the less abundant Paleozoic and the more abundant Mesozoic ophiolites (Alavi, 1991). Stöcklin (1974) divided Iranian ophiolites into four groups: (i) ophiolites of the Zagros; (ii) ophiolites (coloured melanges) of northwestern Iran; (iii) ophiolites and coloured melanges that mark the boundaries of the Central and Eastern Iranian micro-continent (Takin, 1972); and (iv) ophiolites at the northern foot of the Alborz range. Alavi (1991) used information from field relations to classify the Iranian ophiolites into three groups: (i) the Proterozoic, which are present as isolated outcrops on the western edge of the central Iranian microcontinent (CIM), (ii) the pre-Jurassic, which are located within the Alborz Range to the north, and (iii) the post-Jurassic, which are the most abundant.

The Neyriz-Kermanshah Ophiolitic Belt in suture zone is a remnant of the Neo-Tethys ocean that was obducted along the Zagros margin. The Kermanshah ophiolite is described as a piece of Tethyan oceanic lithosphere scraped off during NE-directed subduction underneath the Iranian block (e.g. Braud, 1970, 1978).The Kermanshah ophiolitic complex in western Iran, with about 200km length and 30-60 km wide is part of the High Zagros situated between the Zagros Folded Belt and Sanandaj-Sirjan Zone (Fig. 2) that has not been studied much .The presence of scattered dikes with island arc tholeiite (IAT) affinity is reported by Desmons and Beccaluva (1983). Age of Kermanshah ophiolite (similar to other ophiolite East Mediterranean-Zagros-Oman) is considered by K-Ar method versus 86.3±7.8 and 81.4±3.8 Ma (Delaloye and Desmons, 1980; Braud, 1987).Some diabasic dikes yield $^{40}K/^{40}Ar$ ages of 83–86 Ma (Delaloye and Desmons, 1980). Reported mantle peridotites, gabbro and both island arc tholeiitic and alkaline lavas (Ghazi and Hassanipak, 1999). Recently Allahyari *et al*. (2010) described mantle peridotite, normal mid-ocean ridge basalt (N-MORB) to enriched mid-ocean ridge basalt (E-MORB)-type gabbroic sequences and scarce pillow lavas at Sahneh (NE of Kermanshah).

The Noorabad ophiolite is an important part of Kermanshah ophiolite (Fig. 3) that the results of petrological and geochemical studies of this ophiolite presented in this paper.The goal of this paper is to use field data, petrographic study and geochemical data, including REE and incompatible trace element data for: (i) identify different lithologic units of this complex, (ii) to make clear assessments for the genesis of Noorabad-Kermanshah ophiolites, and (iii) to determine the possible tectonic setting and geodynamic evolution of thisophiolite within the context of the Neo-Tethyan tectonic reconstruction models of Iran and the Middle Eastern region.

2–Regional geology

The Noorabad ophioliteis part of the High Zagros that situated between the Zagros Folded Belt and Sanandaj-Sirjan Zone (Fig 2).In this area the Zagros Fold belt is consists Cretaceous limestone and Pliocene conglomerates (Bakhtiari Formation) which were strongly folded. The internal Sanandaj–Sirjan zone (Stöcklin,1968) made of mainly Jurassic, interbedded phyllites and metavolcanics showing a moderate metamorphic imprint except close to large-scale Mesozoic calc–alkaline plutons (Agard *et al*., 2005; Ahmadi Khalaji *et al*., 2007; Tahmasbi*et al*., 2010;

Shahbazi *et al*., 2010). The high Zagros unit (or Crush Zone) has three separate sub-units, which are consist the Biston limestone (Upper Cretaceous-Lower Triassic), the Kermanshah ophiolite, and the Bakhtaran radiolarite (Aghanabati, 1978, 1990).

Table 1) Major and trace element contents from diabasic dikes and andesitic-basaltic lavas in Noorabad-Kermanshah ophiolite.

Rocktype	B	B	B	B	B	B	D	D	D	D	D	D	A	A	A	A	A	A	A
Sample	B-01	B-02	NK-01	NK-02	NK-11	NK-28	D-01	D-02	D-03	N-06	NK-27	NK-34	T-01	T-02	T-03	NK-18	NK-19	NK-21	NK-22
SiO_2	50.4	51.1	51.3	50.9	51.2	50.6	50.90	51.70	49.20	50.45	51.50	49.20	60	57	57.3	60.1	56.4	59	61.5
TiO_2	0.70	1.04	0.60	0.64	1.41	1.01	1.43	1.18	0.61	0.72	1.39	1.13	0.1	0.3	0.09	0.04	0.24	0.1	0.05
Al_2O_3	12.89	12.96	14.13	13.77	10.50	13.28	15.22	14.35	13.17	14.19	13.57	14.39	13	9.1	10.9	11.8	10.5	11	13.5
Fe_2O_3	9.78	7.37	10.93	11.77	15.90	6.59	8.93	9.35	11.20	11.55	9.25	8.20	8.8	12	11.2	4.36	11.8	11	5.65
MnO	0.10	0.23	0.10	0.09	0.13	0.16	0.16	0.14	0.20	0.08	0.13	0.12	0.1	0.1	0.08	0.14	0.07	0.1	0.09
MgO	5.71	6.54	5.12	5.92	4.10	5.61	6.80	6.32	6.15	5.34	6.84	6.73	5.6	4	4.43	4.86	4.17	4.8	3.65
CaO	14.84	14.16	10.76	10.92	10.42	16.32	11.52	10.51	12.29	10.90	11.31	13.17	7	9.7	8.53	11.5	10.2	8.2	7.57
Na_2O	2.15	2.36	3.12	3.20	2.60	2.64	2.53	2.29	3.78	3.16	2.30	2.83	2.7	2.3	2.24	2.44	1.33	2.2	2.5
K_2O	0.11	0.79	0.24	0.18	0.46	0.80	0.15	0.28	0.40	0.02	0.10	0.07	0.3	0.9	1.44	0.55	1.26	0.3	1.76
P_2O_5	0.13	0.79	0.23	0.18	0.46	0.80	0.26	0.32	0.20	0.23	0.41	0.30	0.5	0.3	0.29	0.32	0.43	0.4	0.27
LOI	2.00	1.90	2.20	1.80	2.20	2.10	1.85	2.20	2.40	2.25	2.30	2.70	2.5	2.8	2.65	2.3	2.75	2.8	2.9
Total	98.81	99.24	98.73	99.37	99.39	99.92	99.75	98.65	99.59	98.90	99.11	98.84	100	98	99.2	98.4	99.1	99	99.4
Ag	0.01	0.13	0.03	0.04	0.05	0.09	0.1	0.11	0.08	0.03	0.12	0.05	0	0	0.02	0.01	0.02	0	0.02
As	4.7	2.3	0.5	0.7	0.7	4.4	0.9	1	6.5	0.5	1.4	0.6	1	1.5	1.4	0.5	1.8	0.8	0.7
Ba	49.5	160.5	20.8	6.2	6.3	120.7	31.4	31	131	14.1	15.2	7.4	13	23	80.3	23	21.2	23	29.8
Be	0.3	0.9	0.5	0.8	0.9	1.1	0.2	0.7	0.4	0.3	0.5	0.4	0.8	0.9	0.7	0.7	1	0.7	1.4
Bi	0.1	0.1	0.1	0.1	0.1	0.1	0.1	0.1	0.1	0.1	0.1	0.1	0.1	0.1	0.1	0.1	0.1	0.1	0.1
Cd	0.2	0.4	0.06	0.11	0.13	0.4	0.41	0.18	0.32	0.06	0.24	0.14	0.1	0.1	0.05	0.07	0.05	0.1	0.05
Co	25.2	36.1	22.6	21.8	23.6	35	28.5	29.9	34.1	20.4	21.5	22.5	27	27	19.4	8.4	10.3	30	13.6
Cr	107	124	108	25	2	106	2	3	74	15	2	11	66	46	21	4	60	50	25
Cs	0.1	0.8	0.1	0.2	0.1	0.4	0.1	0.1	0.7	0.1	0.1	0.3	0.6	1.1	0.9	0.6	2.2	0.4	2
Cu	60.9	67.2	38.3	40.5	33.7	86	145	162	89.5	32.1	95.7	62.2	1.4	13	1	0.7	35.1	58	2.7
Hg	0.05	0.05	0.05	0.05	0.05	0.05	0.05	0.05	0.06	0.05	0.05	0.05	0.1	0.1	0.05	0.05	0.05	0.1	0.05
In	0.03	0.05	0.04	0.02	0.05	0.05	0.04	0.05	0.05	0.02	0.04	0.02	0.1	0.1	0.05	0.06	0.05	0.1	0.07
Li	19.9	18.4	0.6	12.3	6.4	18.3	19.4	6.9	10.5	7.7	4.1	7.9	40	21	19.7	21.4	16.5	33	16.1
Mo	0.4	1.1	0.1	0.4	0.7	1	0.7	0.5	0.6	0.3	1.1	1.1	0.4	0.5	0.3	0.4	0.5	0.4	0.3
Nb	0.5	7.6	1.2	1.4	1.7	4.2	3.9	4.2	1.2	1.3	5.5	1.8	0.5	0.5	0.5	0.5	0.5	0.5	0.5
Ni	91.9	93.5	72.4	66.9	6.3	116.7	29.9	26.3	50.6	34.7	28	63.5	46	35	16.9	34.8	19.7	30	11.4
Pb	1	2.1	1	3	2.8	2.5	8.1	2.3	6.4	0.3	3	2	1.3	2.9	2.3	1.4	1.8	2.3	2
Rb	1.9	24.8	1.4	3.3	3	20.5	3.5	8.8	7.9	0.3	2.4	1.6	6	24	30.6	11.7	30.5	6.3	43.1
Re	0.01	0.01	0.01	0.01	0.01	0.01	0.01	0.01	0.01	0.01	0.01	0.01	0	0	0.01	0.01	0.01	0	0.01
S	198	75	50	344	223	138	122	50	817	50	3498	735	50	50	50	71	50	50	50
Sb	0.1	0.1	0.1	0.1	0.1	0.1	0.1	0.1	1.8	0.1	0.2	0.1	0.1	0.2	0.2	0.1	0.1	0.1	0.1
Sc	14	19	12	9	10	26	9	18	17	6	23	9	19	22	13	5	16	20	14
Se	0.27	0.42	0.37	0.26	0.55	0.54	0.54	0.5	0.43	0.27	0.82	0.42	0.3	0.3	0.25	0.3	0.29	0.3	0.26
Sn	5.4	2.6	1.1	1.2	1.9	1.5	1.4	1.2	1.2	1	1.8	1.2	2.1	1.5	1.5	1.1	2.2	1.2	1.7
Sr	98.9	180.4	50.7	33.8	26.6	161.6	66.8	33.4	97.5	30	55.2	52	21	41	40.3	120	17.1	105	28.8
Te	0.2	0.2	0.2	0.2	0.2	0.2	0.2	0.2	0.2	0.2	0.2	0.2	0.2	0.2	0.2	0.2	0.2	0.2	0.2
Th	0.18	7.38	1.87	2.31	0.67	6.71	2.47	2.68	0.27	0.34	3.73	0.92	2.2	1.6	1.88	1.45	2.29	1.1	1.82
Tl	0.1	0.1	0.1	0.1	0.1	0.1	0.1	0.1	0.1	0.1	0.1	0.1	0.1	0.1	0.1	0.1	0.1	0.1	0.1
U	0.11	1.16	0.44	0.81	0.17	1.07	0.55	0.66	0.1	0.05	0.94	0.15	0.5	0.4	0.55	0.37	0.52	0.3	0.35
V	101	126	124	62	187	131	226	190	161	117	204	108	222	190	143	27	220	221	151
W	0.1	0.2	0.1	0.1	0.1	0.3	0.2	0.1	0.1	0.1	0.2	0.1	0.1	0.1	0.1	0.1	0.1	0.1	0.1
Y	15.67	16.38	26.9	12.02	34.21	22.51	21.8	23.4	18.2	21.1	30.71	21.4	27	17	18.2	15	18.9	23	14.4
Zn	52	118.9	56.9	56.7	114.3	120.8	101	106	136	49.8	108	79	36	23	24.1	19.8	20.9	91	16.6
Zr	44	82	9	52	48	112	38	91	13	16	162	50	8	15	7	8	11	8	13
Ce	7.95	73.41	22.7	19.66	30.13	74.29	36.1	39	19.1	22	58.34	31	58	37	48.5	41.2	38.5	38	37.1
Dy	4.06	4.82	5.59	3.73	8.31	4.88	6.47	6.7	4.66	5.93	9.53	7.9	8.1	5.6	5.89	4.9	6.48	6.4	5.89
Er	2.63	2.45	3.5	2.2	5.33	2.47	4.17	4.2	2.79	3.49	6.01	5.13	4.8	3.1	3.57	2.82	3.68	3.9	3.51
Eu	0.97	2.21	1.33	1.02	1.92	2.22	1.78	1.88	1.3	1.63	2.46	1.86	2	1.7	1.56	1.21	1.5	1.6	1.25
Gd	3.78	7.1	5.52	3.77	8.37	7.31	6.63	7.01	4.8	6.11	9.61	7.68	9.3	6.7	6.76	5.84	7.2	6.9	6.38
Ho	0.98	1.01	1.33	0.87	2.01	1	1.54	1.57	1.05	1.35	2.23	1.88	1.8	1.3	1.39	1.06	1.44	1.5	1.31
La	2.52	49.8	9.73	8.7	11.71	61.44	17.3	17.8	7.96	8.94	28.07	12.3	25	16	22.4	21.8	16.1	16	16.4
Lu	0.66	0.35	0.48	0.35	0.85	0.33	0.68	0.67	0.4	0.53	0.97	0.86	0.7	0.5	0.55	0.48	0.52	0.6	0.55
Nd	7.79	38.73	15.2	11.71	22.28	42.64	20.7	22.4	13.1	16.4	32.46	21.6	34	22	26.6	19.9	23.9	24	21.1
Pr	1.36	9.58	3.12	2.5	4.4	10.68	4.51	4.88	2.6	3.2	7.07	4.36	7.4	4.8	5.98	4.75	5.11	5	4.68
Sm	2.5	6.85	4	2.89	6.03	7.09	5.03	5.42	3.48	4.52	7.5	5.75	7.8	5.3	5.68	4.55	5.87	5.6	4.99
Tb	0.64	0.93	0.9	0.6	1.32	0.92	1.04	1.07	0.74	0.98	1.53	1.27	1.4	1	1.01	0.85	1.09	1.1	0.98
Tm	0.49	0.4	0.61	0.39	0.97	0.42	0.76	0.77	0.48	0.63	1.11	0.96	0.8	0.5	0.63	0.51	0.63	0.7	0.63
Yb	2.66	2.1	3.25	2.17	5.32	2.09	4.16	4.19	2.58	3.42	6.1	5.23	4.6	2.9	3.46	2.91	3.22	3.7	3.48
Nb/Y	0.03	0.46	0.04	0.12	0.05	0.19	0.18	0.18	0.07	0.06	0.18	0.08	0.02	0.03	0.03	0.03	0.03	0.02	0.03
Y/Nb	31.34	2.16	22.39	8.59	20.12	5.36	5.58	5.57	15.13	16.22	5.58	11.87	54.30	34.58	36.40	29.92	37.72	46.94	28.70
Zr/Nb	88.00	10.79	7.50	37.14	28.24	26.67	9.74	21.67	10.83	12.31	29.45	27.78	16.00	30.00	14.00	16.00	22.00	16.00	26.00
Nb/La	0.20	0.15	0.12	0.16	0.15	0.07	0.23	0.24	0.15	0.15	0.20	0.15	0.02	0.03	0.02	0.02	0.03	0.03	0.03
La/Nb	5.04	6.55	8.11	6.21	6.89	14.63	4.44	4.24	6.63	6.88	5.10	6.86	50.94	32.12	44.76	43.58	32.14	32.30	32.76
Nb/U	4.55	6.55	2.73	1.73	10.00	3.93	7.09	6.36	12.00	26.00	5.85	12.00	1.09	1.43	0.91	1.35	0.96	1.79	1.43

Ce/Pb	7.95	34.96	22.70	6.55	10.76	29.72	4.45	16.95	2.99	73.43	19.45	15.51	44.68	12.73	21.08	29.40	21.39	16.57	18.53

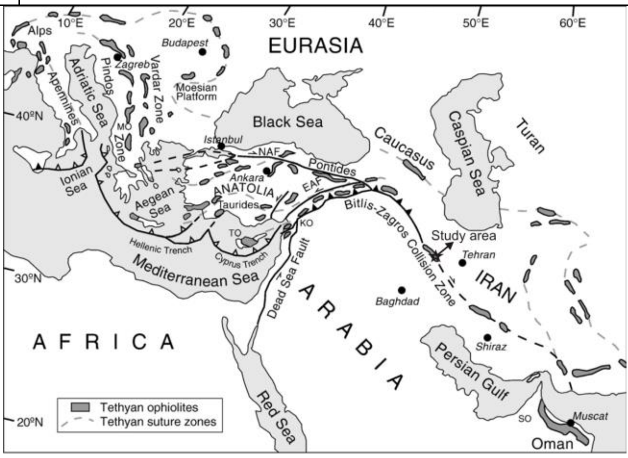

Figure 1) Simplified tectonic map of the eastern Mediterranean region showing the distribution of the Neotethyan ophiolites and suture zones (Dilek et al., 2007).

A part of largely of Kermanshah ophiolite is located around of Noorabad city and is cut by a major SE-NW trending fault. The main rock units in the Noorabad area include rocks of ophiolitic complex, sedimentary rocks and marble (Fig. 3). This ophiolite consist of serpentinized peridotites and pegmatite gabbros as mantle sequence whereas crustal sequences is composed of locally layered gabbros, isotropic gabbros, sheeted dike complex, basaltic to andesitic lavas and sedimentary rock (radiolarites and late Cretaceous pelagic limestones) (Fig. 3).

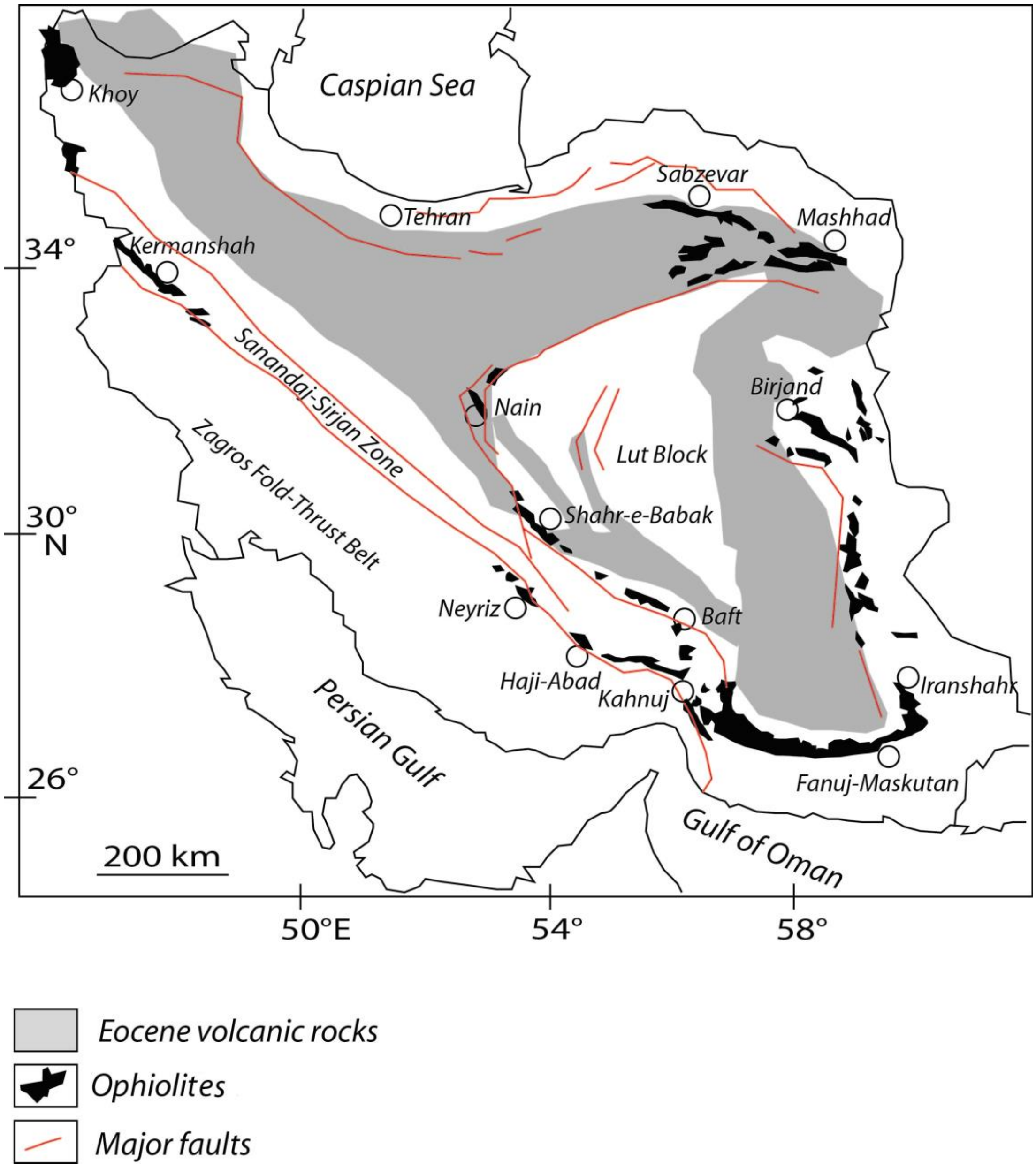

Figure 2) Map showing locations of major Iranian ophiolites (Kiani et al., 2014).

The serpentinized peridotites including dunite, harzburgite and lherzolite are that can be found along the Harsin to Noorabad road and covered by Oligo- Miocene limestone. The Gabbros located in NW parts of the study area consist of isotropic and cumulate gabbros that somewhat are layered in some areas. A well-preserved volcanic sequence (including andesites, basaltic lavas and pillowed basalts) and sheeted dike complex are found in many places (e.g. S of Aleshtar, E of Harsin and around of Noorabad). In more these are as sheeted dikes intruded into basaltic lavas and covered by Bakhtiari formation (Pliocene). Extrusive rocks of the Noorabad Ophiolite are consist of basalt and andesite occurred as hills, and are present as massive flows and blocky outcrop. These rocks show the effects of extensive sub-seafloor hydrothermal alteration and low-grade hydrothermal metamorphism. The basalts of this ophiolite divided into two types: (1) pillow lava (2) spilites basalts that can be found around of Noorabad city.

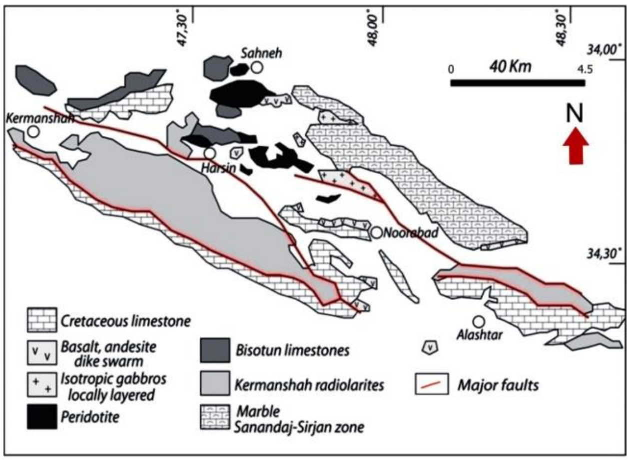

Figure 3) Geologic map of the Kermanshah ophiolitic complex (Kiani et al., 2014).

The Kermanshah radiolarites belongs to an important siliceous complex of Mesozoic age.This sedimentary pile was deposited in a long and narrow basin (Dercourt *et al*., 1993; Ricou and Marcoux, 1980; Ricou *et al*., 1977). This sedimentary basin was part of the Tethyan Ocean and bordered the eastern edge of Gondwana. It extended from the Hawasina region (Oman) in the south, through Pichakun (South Iran, Neyriz series) and Kermanshah (western Iran), and ended in the Kocali basin (Turkey). The Kermanshah radiolarites have two ages consist as Lower Pliensbachian for the oldest ones, up to Turonian for the youngest (Gharib and Wever, 2010).

3–Petrography

The sheeted dikes of the Noorabad ophiolites show the effects of extensive sub-seafloor hydrothermal alteration. These rocks are composed of clinopyroxene (30-40%), plagioclase (40-50%), and opaque minerals (10-20%). These rocks have intergranular, microgranular and poikilitic textures (Fig. 4A). A few samples show vesicles filled with secondary mineral such as chlorite, prehnite, and zeolites(Fig. 4B).The plagioclase laths (1–3 mm in size) altered to sericite and have compositional zoning. The clinopyroxene (1-2mm average size) is generally augite that on effect uralitized process altered to amphibole mineral. The opaque minerals are including pyrite and titanomagnetite altered to iron oxides. The pillow lavas have microvesicles filled with chlorite, carbonates and opaque minerals in a groundmass of plagioclase and clinopyroxene microlites (Fig. 4C). The spilitic basalts have plagioclase (60-70%), clinopyroxene (20-30%) and minor opaque minerals (10-20%) (titaniferous minerals) (Fig. 4D). The clinopyroxenes (1mm or less in length) of these rocks are uralitized and plagioclases (0.5-3mm long) altered into sericite. These rocks have intersertal, aphanitic, porphyritic and variolitic textures. The titaniferous minerals (<1mm) have skeletal texture and altered to iron oxides. Andesites of Noorabad ophiolite in hand specimen and thin section have phenocrysts of plagioclase (60-70%) in a groundmass of clinopyroxene (10-20%) and opaque minerals (20-30%). In these rocks the primary minerals (plagioclase and pyroxene) of rocks altered to secondary minerals (chlorite, sericite, quartz, zeolite and Fe-Oxide). The microvesicles of these rocks are filled with secondary minerals consist sericite, quartz, zeolite, chlorite and opaque minerals. The plagioclases (2-3mm average size) are euhedral to subhedral that shows evidences of fracture and breakage. These rocks have glomeroporphyritic and porphyritic texture (Fig. 4E). The opaque minerals in the alteration zones consist of pyrite, bornite, malachite, azurite and Fe-Oxide (Fig. 4F).

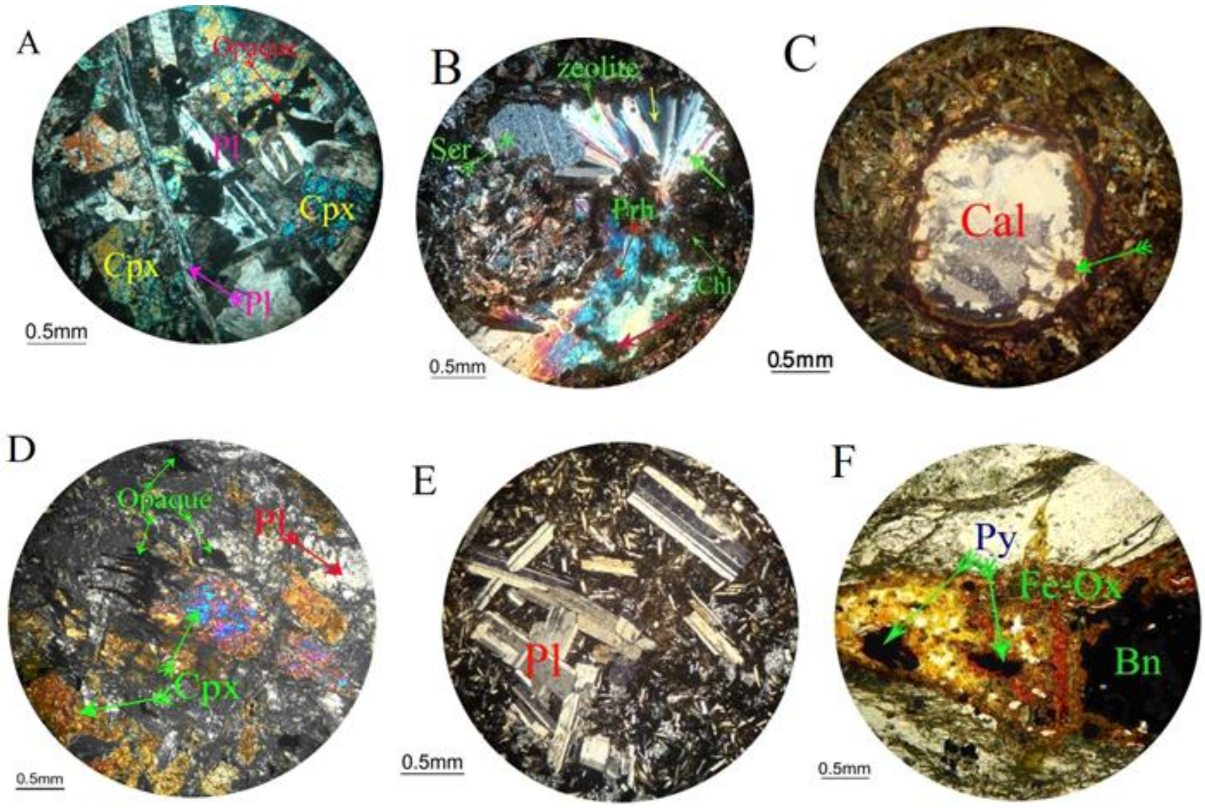

Figure 4) Microphotographs of representative samples (crossed polarized light) :(A) sheeted dikes; (B) vesicles filled with secondary mineral such as chlorite, prehnite, and zeolites in the sheeted dikes; (C) variolitic texture in the pillow lavas; (D) spilitic basalts; (E) glomeroporphyritic texture in the andesite; (F) The opaque minerals (pyrite, bornite and Fe-Oxide) in the andesite. [Pl = plagioclase; Cpx= clinopyroxene; Chl= chlorite; Prh= prehnite; Cal= calcite; Bn = bornite; Fe-Ox = Fe-Oxide; py = pyrite.]

4–Analytical methods

For chemical analysis 19fresh samples (6 samples of basaltic lava, 6 samples of dikes and 7 samples of andesites) from Noorabad ophiolite were analyzed for major, trace and rare earth elements (REE) in Labwest Minerals Analysis Laboratory, Australia (Table 1). Major elements were determined by ICP-AES; in this method 15 gr subsample of the analytical pulp is fused with lithium metaborate at 1000° C and dissolved in nitric acid then determined by ICP-AES. For trace elements and rare earth element (REE) 2gr of sample is digested in a mixture of acids in a microwave digestion system then elemental concentrations are determined by ICP-MS.

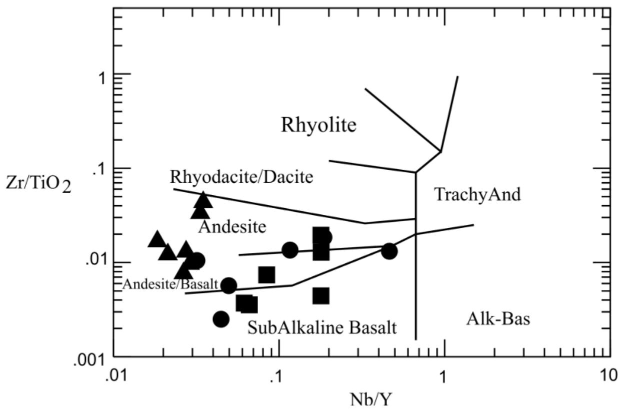

Figure 5) Zr–Ti–Nb–Y geochemical discrimination diagram (Winchester and Floyd (1977) showing three types of lavas and dikes. Solid squares= diabas, Solid circles=basalts and Solid triangles= Andesites.

4.1- Geochemistry

The basaltic extrusive rocks of the Noorabad ophiolite in generally underwent sea-floor alteration and low-grade hydrothermal metamorphism. This alteration typically results in losses or gains of most of the major elements such as alkali and alkali earth elements. Thus, some of the discrimination diagrams, such as alkali-silica and AFM diagrams (Middlemost, 1977; Irvine and Baragar, 1971), which use major element oxides for characterizing chemical types are not useful.

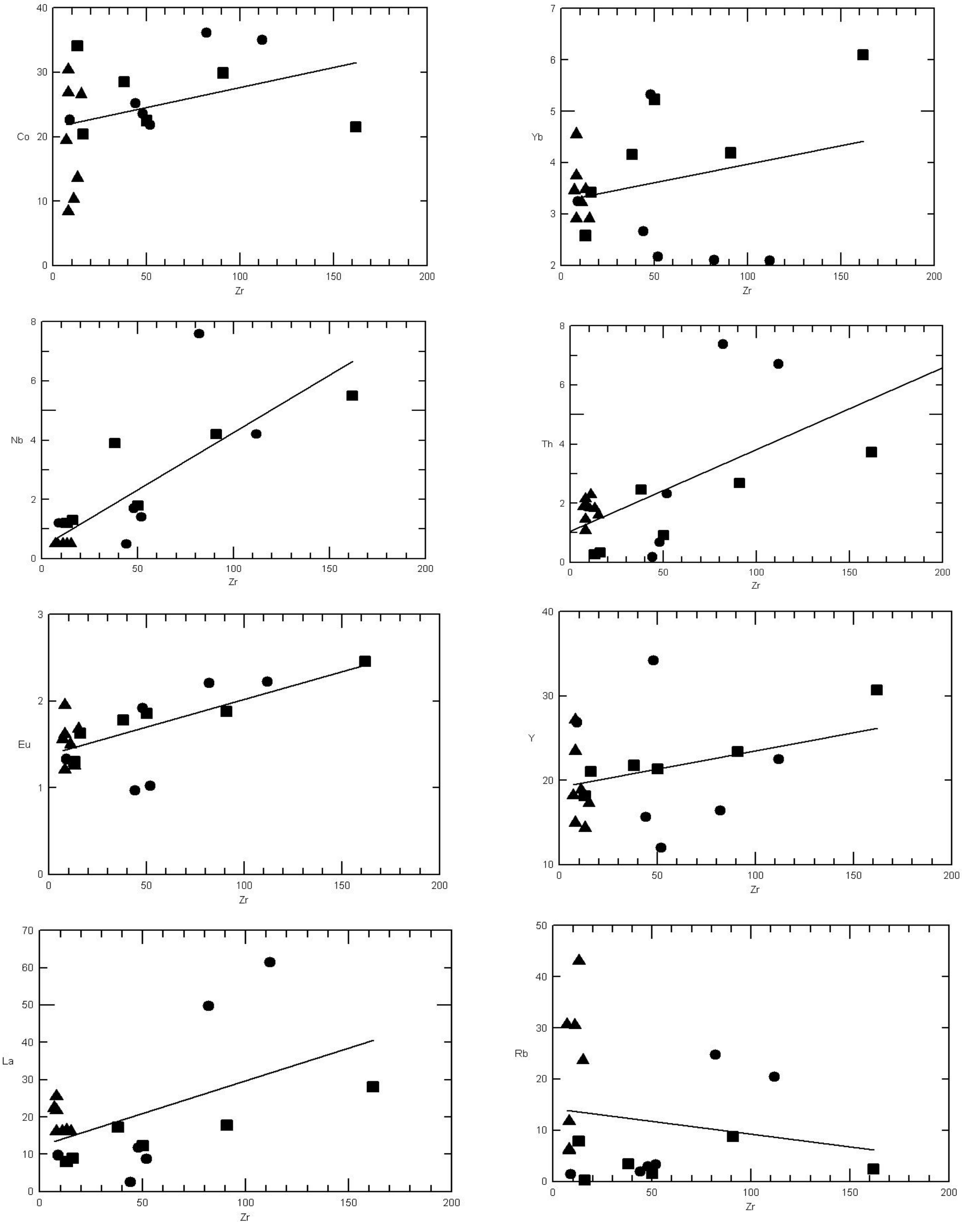

Figure 6) Nb/Y vs. Zr/P_2O_5 diagram with field after delineated after Floyd and Winchester (1975). Symbols as in Fig. 5.

Therefore, in this paper selected minor and trace elements (e.g., Ti, Zr, Y and Nb) that are believed to be relatively immobile under conditions of metasomatism and low-grade hydrothermal metamorphism are used to characterize such basalts with respect to original composition and possible tectonic environment of formation (e.g., Pearce and Cann, 1973; Winchester and Floyd, 1977; Pearce, 1996; Jenner, 1996).

The Lavas (basalts and andesites) and dikes of this ophiolite have lower TiO_2 (0.04-1.43%) contents and exhibit enrichment in large-ion lithophile elements(LILE) such as Ba, Rb, K, and Th relative to high-field strength elements (HFSE) such as Ti, Zr, Nb, Y and such enrichment of LREE relative to HREE (except B.1 sample) suggest arc magmas affinities (e.g. Pearce 1982; Shervais 1982; Pearce and Peate1995).These differences are generally attributed to the addition of a hydrous fluid from the subducting slab to the overlying mantle wedge (Pearce and Peate 1995).

On the Nb/Y–Zr/Ti discrimination diagram (Winchester and Floyd, 1977) the lavas (basalts and andesites) and dikes from the Noorabad ophiolite plot in the sub-alkaline field. These rocks divided into basalt, andesite-basalt and andesite (Fig. 5). On the Nb/Y vs. Zr/P_2O_5 diagram (Floyd and Winchester, 1975), these rocks plot in the tholeiite field (Fig. 6). Trace elements versus Zr diagrams are illustrated in Fig. 7. Most of the samples display near-linear to curvilinear trends of increasing with increasing Zr content. In La-Y-Nb discrimination diagram (Cabanis and Lecolle, 1989) all samples plot in island arc basalts fields (Fig. 8). In Th-Zr-Nb discrimination diagram of Wood (1980), all the samples plot within the subduction zone (SSZ) field (Fig. 9). In this diagram, all samples show depletion in Nb and Hf (Fig. 9). On the Th/Yb versus Nb/Yb ratio plots (Pearce 1982; Pearce *et al*., 1995) all samples plot in the subduction zone field (Fig. 10).

Patterns normalized to NMORB for all samples are depleted in Sr, Ba and K, suggesting theextensive mobility of these elements during sub-sea-floor hydrothermal metamorphism (e.g., Pearce and Cann, 1973; Winchester and Floyd, 1977; Pearce, 1996; Jenner, 1996; Harper *et al*., 1988; Harper, 1995).

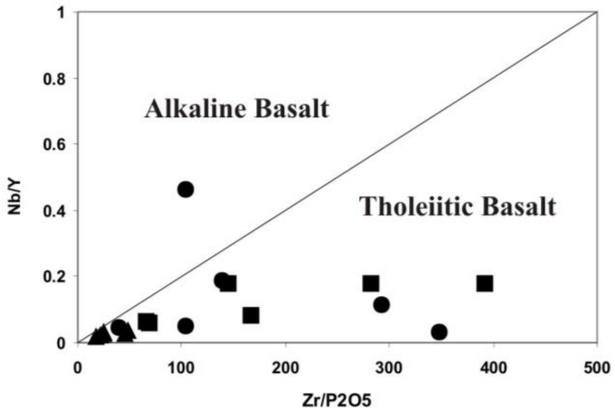

Figure 7) Trace elements versus Zr diagrams. Symbols as in Fig. 5.

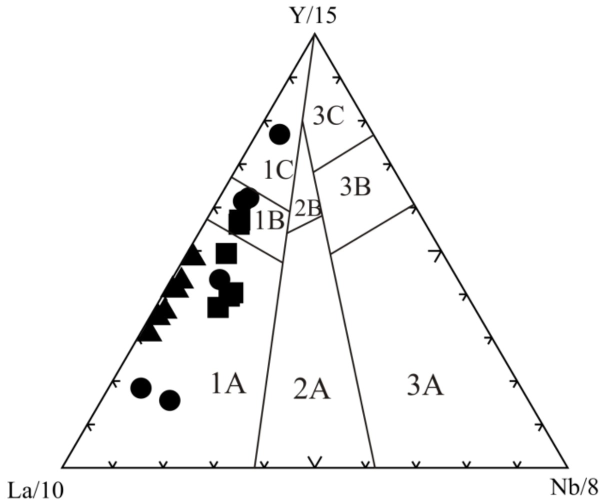

Figure 8) La-Y-Nb discrimination diagram (Cabanis and Lecolle, 1989) that show all samples plot in island arc basalts fields. Field 1 contains volcanic-arc basalt, field 2, continental basalt, and field 3, oceanic basalt. The subdivisions of the fields are as follows: 1A, calc-alkalic basalt; 1B, calc-alkalic basalt and volcanic arc tholeiite; 1C, volcanic arc tholeiite; 2A, continental basalt; 2B, back-arc basin basalt; 3A, alkalic basalt from intercontinental rift; 3B + 3C, E-type MORB (3B enriched; 3C weakly enriched); and 3D, N-type MORB. (Symbols are similar to Fig. 5).

According to patterns normalized to NMORB, more dibasic dikes are enriched as basaltic rocks of large-ion lithophile elements (LILE) Such as Pb, Rb, Cs, U and Th ($Th_{(n)}/La_{(n)}$=1.2) and is depleted in High Field Strength Elements (HFSE) such as Ti, Nb, Zr and Y ($Nb_{(n)}/La_{(n)}$=0.14-0.23). Of course these rocks are depleted in Ba, K and Pb (Just in case D-3) due to alteration (Fig. 11A).

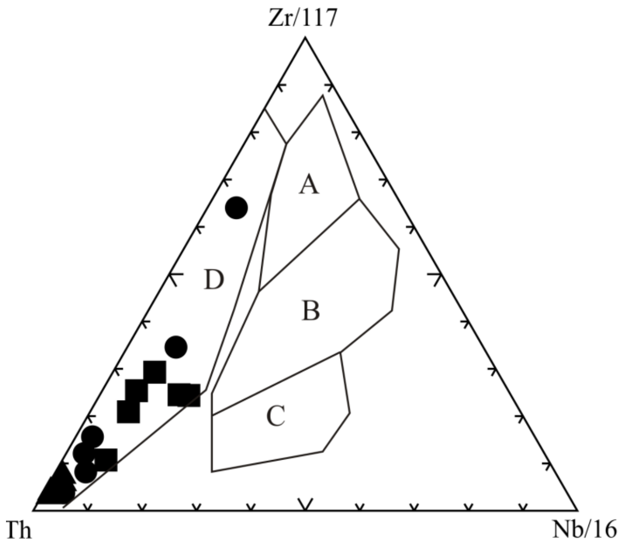

Figure 9) Th-Zr/117-Nb/16 discrimination diagram (Wood, 1980) showing that all the sampels plot within the supra-subduction zone (SSZ) field. (A) N-MORB type, (B) E- MORB type and tholeiitic basalt within plate and differentiates, (C) alkaline within plate basalt and within the plate basalts and differentiates, (D) destructive plate-margin basalts and differentiates (subduction zone).(symbols are similar to Fig. 5).

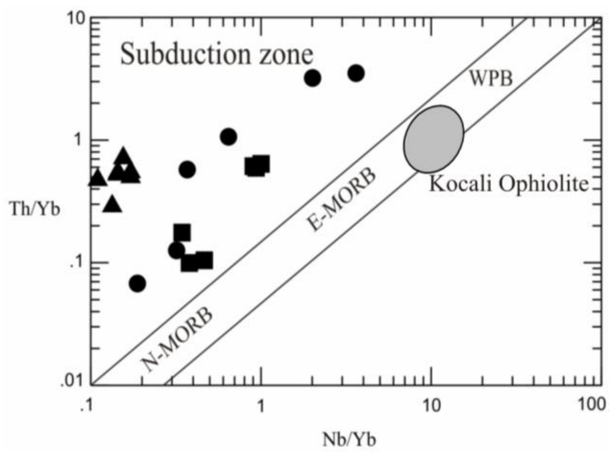

Figure 10) Th/Yb versus Nb/Yb diagram (Pearce and Peate, 1995) showing that all the sampels plot within the subduction zone field. Shaded areas show the field of Kocali ophiolite (Varol et al., 2011). (symbols are similar to Fig. 5).

Chondrite- normalized spider diagrams show that diabase dikes are enriched in LREE relative to HREE elements ($La_{(n)}/Yb_{(n)}$=1.7-3.3) (Fig. 11B). Enrichment of light rare earth elements (LREE) and heavy rare earth elements depletion (HREE) in this diabasic dike are associated with significant calc-alkaline magma series of volcanic arc (Monnier *et al*., 1995).

NMORB normalized diagrams for pillow lavas show that these rocks are enriched in large-ion lithophile elements (LILE) such as Pb, Rb, K, Cs, U and Th ($Th_{(n)}/La_{(n)}$=2.1) and high field strength elements (HFSE) such as Ti, Nb, Zr and Y ($Nb_{(n)}/La_{(n)}$=0.07-0.2)(Fig. 12A). Negative anomalies of Nb and enrichment in LILE relative to HFSE are typical characteristics of subduction-related magmas) Rolland, 2000; Kelemen *et al*., 1993). REE patterns (spider diagram normalized to chondrite) for basalts Noorabad shows three different trends (Fig. 12B): 1) NK-28 and B-2 Samples are enriched in light rare earth elements (LREE) than heavy rare earth elements (HREE) ($La_{(n)}/Yb_{(n}$=17-21). This pattern is similar to series of basalt and calc-alkaline magma produced in a subduction zone and also is similar to Neyriz ophiolite basalts (Sarkarinejad, 1994) and Nain-Baft opiolite calc- alkaline lavas (Shafaii Moghadam *et al*, 2009).2) NK-1, NK-11andNK-2 examples have patterns almost flat to slightly enriched in LREE ($La_{(n)}/Yb_{(n)}$)=1.6-2.9) that is characteristics of intermediate rocks between tholeiitic series and calc–alkaline in island arc. 3) B.1 sample is depleted in LREE relative to HREE elements ($La_{(n)}/Yb_{(n)}$ = 0.7) that is indicative orientate to the N-MORB-type basalts, although Nb depletion observed in this sample indicates tholeiitic trend.

Patterns normalized NMORB for the andesites show that rocks are enriched in LILE as Cs, U ($Th_{(n)}/La_{(n)}$=0.54-1.15) and Th and depleted in HFSE as Nb, Zr and Ti ($Nb_{(n)}/La_{(n)}$=0.01-0.03)(Fig. 13A).

Chondrite normalized spider diagrams show that andesites are enriched in LREE relative to HREE elements) $La_{(n)}/Yb_{(n)}$=3.1-5.3)(Fig. 13B). Enrichment of LREE and LILE and depletion of HREE and HFSE in these rocks is similar to pillow lavas and diabasic dike that can be attributed a common source for all rocks.

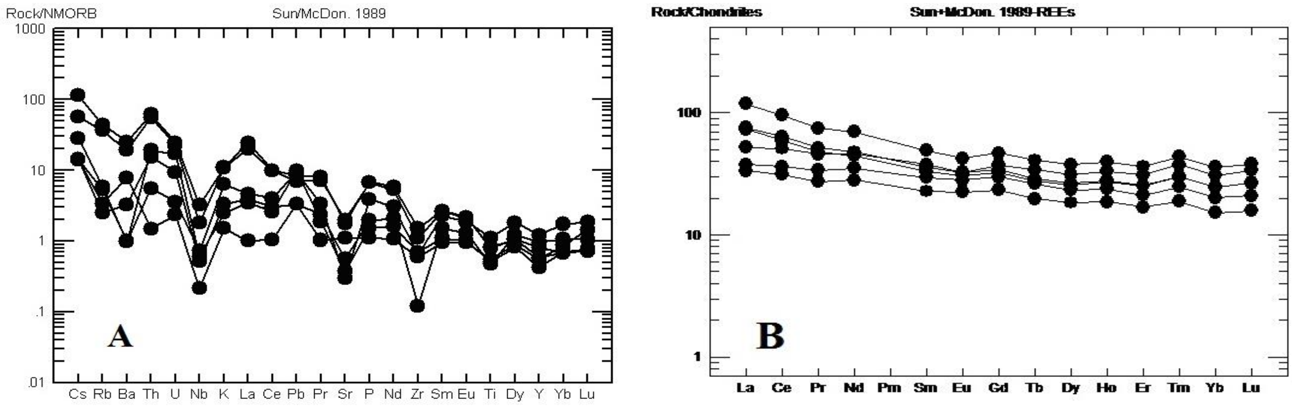

Figure 11) NMORB normalized and chondrite normalized patterns (Sun and McDonough, 1989) for diabasic dikes from Noorabad ophiolite. (Symbols are similar to Fig. 5).

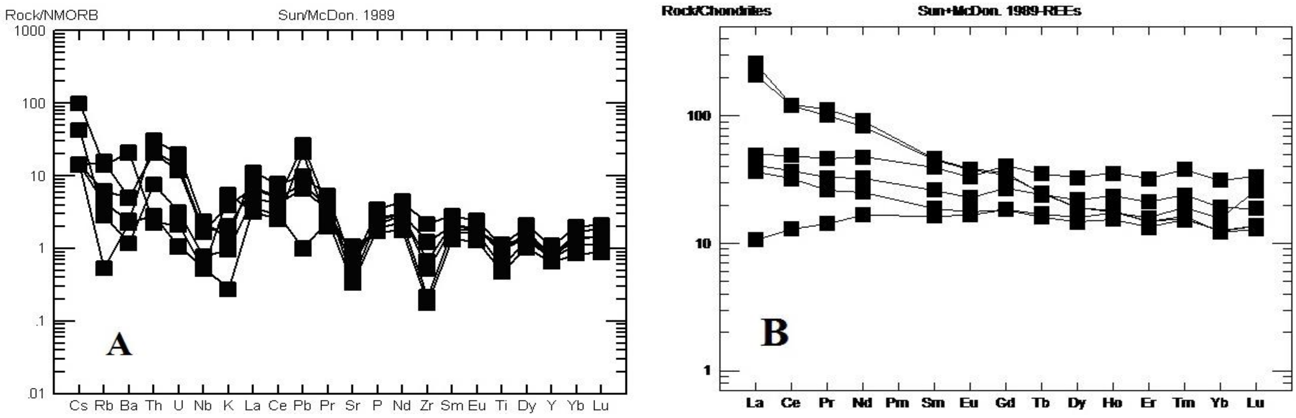

Figure 12) NMORB normalized and chondrite normalized patterns (Sun and McDonough, 1989) for basaltic lavas from Noorabad ophiolite. (Symbols are similar to Fig. 5).

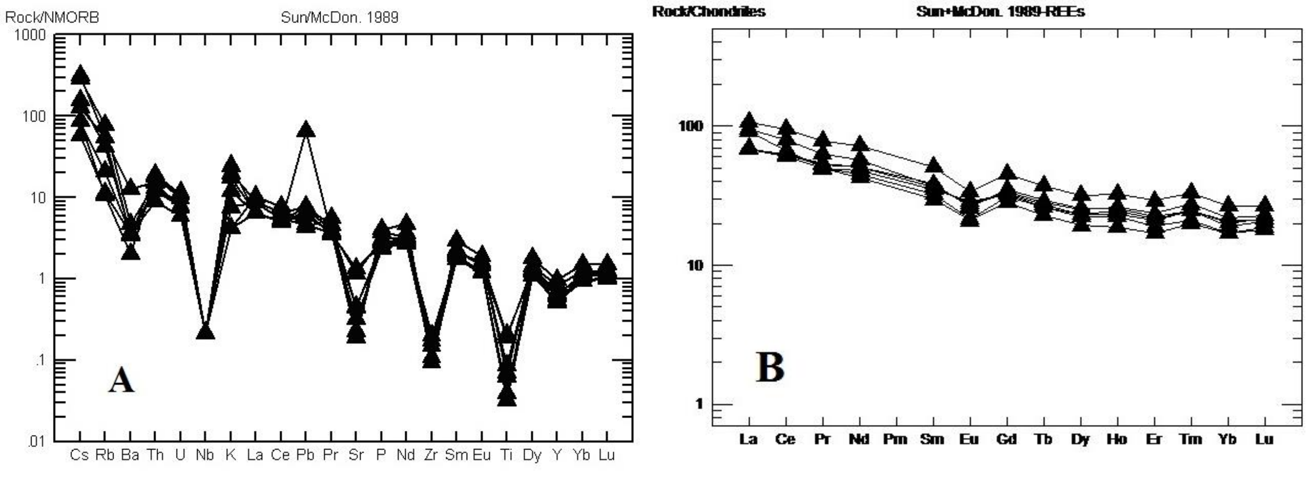

Figure 13) NMORB normalized and chondrite normalized patterns (Sun and McDonough, 1989) for andesites from Noorabad ophiolite. (Symbols are similar to Fig. 5).

5–Discussion andConclusions

The Noorabad- Kermanshah ophiolite is part of Eastern Mediterranean-Zagros-Oman Tethyan ophiolites, cropping out in south-southwest of the Main Zagros Thrust fault. In thissequenceoftheophioliterocks, diabasicdikes,basaltand andesitearewidespread. These rocks show the effects of extensive sub-seafloor hydrothermal alteration. In these rocks the primary minerals (plagioclase and pyroxene) altered to secondary minerals(chlorite, sericite, quartz, zeolite andFe-Oxide). Mineralization in the andesitesis: chalcopyrite, bornit, pyrite, malachite, chalcocite, covellite, azurite and iron-oxide minerals. This mineralizatin is in the alteration zones. Diabasic dikes have intergranular, microgranular and poikilitic textures. The basalts have intersertal, aphanitic, porphyritic and variolitic textures and the andesites have glomeroporphyritic and porphyritic texture. Based on geochemical studies, the studied rocks have common source, calc-alkaline magmas signaturesand are enrichment in LREE and LILE and depletion HFSE elements. These characteristics are similar to other Tethyan ophiolites along the seam suture zone- Zagros (Bitlis-Zagros suture zone) are exposed, and their formation is associated with supra-subduction zones.

Acknowledgments:

The author would like to thank Dr. Z. Tahmasbi, Dr. C. Donmezand Dr. M.I. Kakarfor their appreciate comments which help us to improve manuscript.

References:

Agard, P., Omrani, L., Jolivet, L., Mouthereau F. 2005. Convergence history across Zagros (Iran): constraints from collisional and earlier deformation. International Journal Earth Sciences: 94, 401–419.

Aghanabati, A. 1978. Geological maps of Kermanshah Quadrangle, scale, 1:250,000: Geological Survey of Iran.

Aghanabati, A. 1990. Explanatory text of the Bakhtran quadrangle map 1:250,000. A translation from French by Braud J. Geological Survey of Iran, Geological Quadrangle No. C6.

Ahmadi-Khalaji, A., Esmaeily, D., Valizadeh, M.V., Rahimpour-Bonab, H. 2007. Petrology and geochemistry of the granitoid complex of Boroujerd, Sanandaj-Sirjan Zone, Western Iran. Journal of Asian Earth Sciences: 29, 859–877.

Alavi, M. 1991. Tectonic Map of the Middle East. Geological Survey of Iran.

Allahyari, K., Saccan, E., Pourmoafi, M., Beccaluva, L., Masoudi, F. 2010. Petrology of mantle peridotites and intrusive mafic rocks from the Kermanshah Ophiolitic Complex (Zagros Belt, Iran): implications for the geodynamic evolution of the Neo-Tethyan oceanic branch between Arabia and Iran. Ofioliti: 35, 71–90.

Arvin, M. 1990. Petrology and geochemistry of ophiolites and associated rocks from the Zagros suture, Neyriz, Iran. In: Malpas, J., Moores, E.M., Panayiotou, A., Xenophontos, C. (Eds.), Ophiolites, Oceanic Crustal Analogues. Proceedings of the Symposium “Troodos 1987”. Geological Survey Department, Nicosia, Cyprus, 351–365.

Braud, J. 1970. Les formations du Zagros dans la region de Kermanshah (Iran) et leurs rapports structuraux. Comptes Rendus l’Academie des Sciences: 271, 1241–1244.

Braud, J. 1978. Geological Map of Kermanshah, 1/250000: Geological Survey of Iran.

Cabanis, B., Lecolle, M. 1989. Le diagramme La/10-Y/15-Nb/8: un outil pour la discrimination des series volcaniques et la mise en evidence des processus de melange et/ou de contamination crustale. Comptes Rendus de l'Académie des Sciences - Series II, 2023–2029.

Delaloye, M., Desmons, J. 1980. Ophiolites and mélange terranes in Iran: a geochronological study and its paleotectonic implications. Tectonophysics: 68, 83–111.

Dercourt, J., Ricou, L. E., Vrielynck, B. 1993. Atlas Tethys Paleoenvironmental maps. Gauthier Villars: 307.

Desmons, J., Beccaluva, L. 1983. Mid-ocean ridge and islandarc affinities in ophiolites from Iran: palaeographic implications. Chemical Geology: 39, 39–63.

Dilek, Y., Delaloye, M. 1992. Structure of the Kizildag ophiolite, a slow-spread Cretaceous ridge segment north of the Arabian promontory. Geology: 20, 19–22.

Dilek, Y., Furnes, H., Shallo, M. 2007. Suprasubduction zone ophiolite formation along the periphery of Mesozoic Gondwana. Gondwana Research: 11, 453–475.

Dilek, Y., Furnes, H., Shallo, M. 2008. Geochemistry of the Jurassic Mirdita Ophiolite (Albania) and the MORB to SSZ evolution of a marginal basin oceanic crust. Lithos: 100, 174–209.

Dilek, Y., Moores, E.M. 1987. Regional tectonics of the eastern Mediterranean ophiolites. In: Malpas, J., Moores, E.M., Panayiotou, A., Xenophontos, C. (Eds.), Ophiolites, Oceanic Crustal Analogues. Proceedings of the Symposium ``Troodos 1987''. Geological Survey Department, Nicosia, Cyprus: 295–309.

Floyd, P. A., Winchester, J. A. 1975. Magma Type and Tectonic Setting Discrimination using immobile trace elements. Earth and Planetary Science Letters: 27, 211–218.

Gharib, F., De Wever, P. 2010. Mesozoic radiolarians from the Kermanshah formation (Iran). Comptes Rendus Palevol: 9, 209–219.

Ghazi, A.M., Hassanipak, A.A. 1999. Geochemistry of subalkaline and alkaline extrusives from the Kermanshah ophiolite, Zagros Suture Zone, western Iran: implications on Tethyan plate tectonics. Journal of Asian Earth Sciences: 17, 319–332.

Harper, G.D. 1995. Pumpellyosite and prehnitite associated with epidosite in the Josephine ophiolite-Ca metasomatism during upwelling of hydrothermal fluids at a spreading axis. In: Schiffman, P.,Day, H. (eds) Low Grade Metamorphism of Mafic Rocks. Geological Society of America, Special Papers: 296, 101–122.

Harper, G.D., Bowman, J. R., Kuhns, R. 1988. Field, chemical, and isotopic aspects of submarine hydrothermal metamorphism of the Josephine ophiolite, Klamath Mountains, California-Oregon. Journal of Geophysical Research: 93, 4625-4657.

Hassanipak, A.A., Ghazi, A.M. 2000. Petrology, geochemistry and tectonic setting of the Khoy ophiolite, northwest Iran: implications for Tethyan tectonics. Journal of Asian Earth Sciences: 18, 109–121.

Hébert, R., Huot, F., Wang, C., Liu, Z. 2003. Yarlung Zangbo ophiolites (Southern Tibet) revisited: geodynamic implications from the mineral record. In: Dilek, Y., Robinson, P.T. (Eds.), Ophiolites in Earth History. Geological Society of London Special Publication: 218, 165–190.

Hebert, R., Laurent R. 1989. The mineralogical study of a cross-section through the plutonic part of the Troodos ophiolite: New constraints for genesis of arc-type ophiolite, in Malpas, J., *et al*., eds., Ophiolites–Oceanic crustal analogues. Proceedings of the Symposium "Troodos 1987": Nicosia, Cyprus Geological Survey: 149–164.

Irvine, T.N., Baragar, W.R.A., 1971. A guide to chemical classification of common volcanic rocks. Canadian Journal of Earth Sciences: 8, 523–547.

Jenner, G.J. 1996. Trace element geochemistry of igneous rocks: geochemical nomenclature and analytical geochemistry. In: Wyman, D. A. (Ed.). Trace element geochemistry of volcanic rocks: Applications for massive sulphide exploration, Volume 12. Geological Association of Canada, Short Course Notes: 51–78.

Kelemen, P. B., Shimizu, N., Dunn, T. 1993. Relative depletion of Niobium in some arc magmas and the continental crust. Earth and Planetary Science Letters: 120, 11–134.

Kiani, M., Panahi, A., Shabani, Z., Moridi, M. M, Bijani, M. H. 2014. Geology, Petrology and Geochemical Dispersion of Elements in Noorabad Ophiolite (Northwest Lorestan), Iran. Journal of Academic and Applied Studies (Special Issue on Applied Sciences): 4, 37–50.

Malpas, J., Zhou, M. F., Robinson, P.T., Reynolds, P.H. 2003. Geochemical and geochronological constraints on the origin and emplacement of the Yarlung Zangbo ophiolites, Southern Tibet. In: Dilek, Y., Robinson, P.T. (Eds.), Ophiolites in Earth History. Geological Society of London Special Publication: 218, 191–206.

Middlemost, E.A.K. 1977. The basalt clan. Earth Science Review: 1, 51–57.

Monnier, C., Girardeau, J., Maury, R.C., Cotten, J. 1995. Back-arc basin origin for the East Sulawesi Ophiolite (eastern Indonesia). Geology: 23, 851–854.

Moores, E.M., Robinson, P.T., Malaps, J., Xenophonotos, C. 1984. Model for the origin of the Troodos massif, Cyprus, and other mid- east ophiolites. Geology: 12, 500–503.

Parlak, O., Hoeck, V., Kozlu, H., Delaloye, M. 2006. Oceanic crust generation in an island arc tectonic setting, SE Anatolian Orogenic Belt (Turkey). Geological Magazine: 141, 583–603.

Pearce, J. A., Cann, J. R. 1973. Tectonic setting of basic volcanic rocks determined using trace element analyses. Earth and Planetary Science Letters: 19, 290−300.

Pearce, J.A. 1982. Trace element characteristics of lavas from destructive plate boundaries. In: THORPE, E.S. (ed.) Andesites. Wiley, New York: 525–548.

Pearce, J.A., 1996. A user's guide to basalt discrimination diagrams. In: Wyman, D.A. (Ed.). Trace element geochemistry of volcanic rocks: Applications for massive sulphide exploration, Volume 12. Geological Association of Canada, Short Course Notes: 79–113.

Pearce, J.A., Baker, P.E., Harvey, P.K., Luff, I.W., 1995. Geochemical evidence for subduction fluxes, mantle melting and fractional crystallization beneath the South Sandwich Island Arc. Journal of Petrology: 36, 1073–1109.

Pearce, J.A., Alabaster, T., Shelton, A.W., Searle, M.P. 1981. The Oman ophiolite as a Cretaceous arc–basin complex: evidence and implications. Philosophical Transactions of the Royal Society of London: 300, 299–317.

Pearce, J.A., Lippard, S.J., Roberts, S. 1984. Characteristics and tectonic significance of supra–subduction zone ophiolites. In: Kokelaar, B.P., Howells, M.F. (Eds.), Marginal Basin Geology. Geological Society of London Special Publication: 16, 77–89.

Pearce, J.A., Peate, D.W. 1995. Tectonic implications of the composition of volcanic arc magmas. Annual Review of Earth and Planetary Sciences: 23, 251–286.

Rampone, E., Piccardo, G.B. 2000. The ophiolite–oceanic lithosphere analogue: new insights from the Northern Apennines (Italy). In: Dilek, Y., Moores, E.M., Elthon, D., Nicolas, A. (Eds.), Ophiolites and Oceanic Crust: New Insights from Field Studies and the Ocean Drilling Program. Geological Society of America Special Paper: 349, 21–34.

Ricou, L.E., Braud, J., Brunn, J.H. 1977. Le Zagros. Mém. Soc. Géol. Fr.: 8, 33–52.

Ricou, L.-E., Marcoux, J. 1980. Organisation générale et rôle structural des radiolarites et ophiolites le long du système alpino-méditerranéen Bulletin Society geology France: 1, 1–14.

Robinson, P.T., Malpas, J. 1990. The Troodos ophiolite of Cyprus: new perspectives on its origin and emplacement. In: Malpas, J., Moores, E.M., Panayiotou, A., Xenophontos, C. (Eds.), Ophiolites, Oceanic Crustal Analogues. Proceedings of the Symposium “Troodos 1987”. The Geological Survey Department, Nicosia, Cyprus: 13–26.

Rolland, Y. 2000. Middle Cretaceous back arc formation and arc evolution along the Asian margin. Tectonophysics: 325, 145–173.

Sarkarinejad, K. 1994. Petrology and tectonic setting of the Neyriz ophiolite, southeast Iran. In: Ishiwatari, A. *et al*. (Eds.) Circum-Pacific Ophiolites. Proceeding of the 29th. International Geological Congress: 221–234.

Shafaii Moghadam, H., Stern, R.J. 2011. Geodynamic evolution of Upper Cretaceous Zagros ophiolites: formation of oceanic lithosphere above a nascent subduction zone. Geological Magazine: 148, 762–801.

Shafaii Moghadam, H., Stern, R. J., Kimura, J.-I., Hirahara, Y., Senda, R., Miyazaki, T. 2012. Hf-Nd Isotopic Constraints on the Origins of Zagros Ophiolites. The Island Arc: 21, 202–214.

Shafaii Moghadam, H., Whitechurch, H., Rahgoshay, M., Monsef, I. 2009. Significance of Nain- Baft ophiolitic belt (Iran): short-lived, transtensional Cretaceous back-arc oceanic basins over the Tethyan subduction zone. Comptes Rendus Geosciences: 341, 1016–28.

Shahbazi, H., Siebel, W., Pourmoafee, M., Ghorbani, M., Sepahi, A.A., Shang, C.K., Vousoughi Abedini, M. 2010. Geochemistry and U-Pb zircon geochronology of the Alvand plutonic complex in Sanandaj-Sirjan Zone (Iran): New evidence for Jurassic magmatism. Journal of Asian Earth Sciences: 39, 668–683.

Shervais, J.W. 1982. Ti-V plots and the petrogenesis of modern and ophiolitic lavas. Earth and Planetary Science Letters: 59, 101–118.

Stöcklin, J. 1968. Structural history and tectonics of Iran: a review. American Association of Petroleum Geologists Bulletin: 52, 1229–1258.

Stöcklin, J. 1974. Possible ancient continental margin in Iran. In: Burke, C.A., Drake, C.L. (Eds.). The Geology of Continental Margins. Springer, New York: 873–887.

Sun, S. S., McDonough, W.F. 1989. Chemical and isotopic-systematics of oceanic basalts: implications for mantle composition and processes. In: Saunders, A.D., Norry, M.J. (Eds.), Magmatism in the Ocean Basins. Geological Society of London Special Publication: 42, 313–345.

Tahmasbi, Z., Castro, A., Khalili, M., Ahmadi-Khalaji, A., Rosa, J. 2010. Petrologic and geochemical constraints on the origin of Astaneh pluton, Zagros orogenic belt, Iran. Journal of Asian of Earth Sciences: 39, 81–96.

Takin, M. 1972. Iranian geology and continental drift in the Middle East. Nature: 235, 147–150.

Tribuzio, R., Tiepolo, M., Vannucci, R., Bottazzi, P. 1999. Trace element distribution within the olivine-bearing gabbros from the Northern Apennine ophiolites (Italy): evidence for post-cumulus crystallization in MOR-type gabbroic rocks. Contributions to Mineralogy and Petrology: 134, 123–133.

Varol, E., Bedi, Y., Tekin U. K., Uzunçimen, S. 2011. Geochemical and Petrological characteristics of Late Triassic basic volcanic rocks from the Kocali complex; SE Turkey: implications for the Triassic Evolution of Southern Tethys. Ofioliti: 36, 101–115.

Winchester, J.A., Floyd, P.A. 1977. Geochemical discrimination of different magma series and their differentiation products using immobile elements. Chemical Geology: 20, 325–342.

Wood, D.A. 1980. The application of a Th-Hf-Ta diagram to problems of tectonomagnetic classification and to establishing nature of basaltic lavas of the British Tertiary Volcanic Province. Earth and Planetary Science Letters: 50, 11–30.